Distributed Coordinated Reactive Power Control for Voltage Regulation in Distribution Networks

Zhiyuan Tang, *Member, IEEE,* David J. Hill, *Life Fellow, IEEE,* and Tao Liu, *Member, IEEE*

***Abstract*—In this paper, a novel distributed coordinated control framework is proposed to handle the uncertain voltage violations in active distribution networks. It addresses the problem of coordination of different types of devices in a distributed manner. In our control design, on-load tap changers (OLTCs) are firstly employed to handle the potential voltage violations based on the prediction of renewable outputs and load variations. During real-time operation, once an unmanageable voltage violation is detected, the reactive power of distributed energy resources (DERs) will be coordinated immediately to provide fast corrective control. The control schedules of OLTCs are calculated by solving a multitime-step constrained optimization problem via the alternating direction method of multipliers, whereas the reactive power injections of DERs are determined by a novel online distributed algorithm. The effectiveness of the proposed control framework is verified on the modified IEEE 34-bus and 123-bus test feeders.**

***Index Terms*—Voltage control, distributed control, reactive power control, distribution network, on-load tap changer.**

NOMENCLATURE

$\boldsymbol{\Delta}$	Diagonal weight matrix for slack vector $\boldsymbol{\delta}$
$\boldsymbol{\lambda}^{max}$	Auxiliary Lagrangian multipliers associated with $\overline{\boldsymbol{\lambda}}$
$\boldsymbol{\lambda}^{min}$	Auxiliary Lagrangian multipliers associated with $\underline{\boldsymbol{\lambda}}$
$\boldsymbol{\mu}^{max}$	Auxiliary Lagrangian multipliers associated with $\overline{\boldsymbol{\mu}}$
$\boldsymbol{\mu}^{min}$	Auxiliary Lagrangian multipliers associated with $\underline{\boldsymbol{\mu}}$
$\boldsymbol{\Phi}$	Diagonal weight matrix for slack vector $\boldsymbol{\varphi}$
$\boldsymbol{\Upsilon}$	Diagonal weight matrix for slack vector $\boldsymbol{\varepsilon}$
$\boldsymbol{\varepsilon}$, $\boldsymbol{\delta}$	Vectors of slack variables with non-negative entries in the first stage
$\boldsymbol{\varphi}$, $\boldsymbol{\xi}$	Vectors of slack variables with non-negative entries in the second stage
$\boldsymbol{\Xi}$	Diagonal weight matrix for slack vector $\boldsymbol{\xi}$
$\boldsymbol{C}$	Diagonal matrix with non-negative coefficients for regulating OLTCs
$\boldsymbol{D}$	Weight matrix for regulating reactive power of DERs
$\boldsymbol{n}^{max}$	Upper tap ratio limits of OLTCs
$\boldsymbol{n}^{min}$	Lower tap ratio limits of OLTCs
$\boldsymbol{p}_i$	Vector of active power injections in CA_i
$\boldsymbol{q}_g$	Vector of reactive power generated by DERs
$\boldsymbol{q}_i$	Vector of reactive power injections in CA_i
$\boldsymbol{R}_i$, $\boldsymbol{X}_i$	System matrices of CA_i
$\boldsymbol{v}$	Set of network bus voltages
$\boldsymbol{v}^{max}$	Upper voltage limits on network buses
$\boldsymbol{v}^{min}$	Lower voltage limits on network buses
$\boldsymbol{v}_i$	Vector of bus voltages in CA_i
$\Delta v_{t_i^i}$	Auxiliary variable assigned to CA_i in ADMM to enforce boundary condition
$\Delta v_{t_{i+1}^i}$	Auxiliary variable assigned to CA_i in ADMM to enforce boundary condition
γ	Step size
λ_i^i, λ_{i+1}^i	Dual variables related to boundary conditions in CA_i
$\mathcal{E}$	Set of line segments
$\mathcal{E}_i$	Set of line segments in CA_i
$\mathcal{N}$	Set of network buses
$\mathcal{N}_b$	Set of load buses
$\mathcal{N}_f$	Set of buses incident to the primary-side of OLTCs
$\mathcal{N}_i$	Set of buses in CA_i
$\mathcal{N}_j^d$	Set of descendant buses of bus j
$\mathcal{N}_s$	Set of buses incident to the secondary-side of OLTCs
$\mathcal{N}_t$	Set of virtual secondary-side bus of OLTCs
$\overline{\boldsymbol{\lambda}}$, $\underline{\boldsymbol{\lambda}}$	Lagrangian multipliers related to voltage inequalities
$\overline{\boldsymbol{\mu}}$, $\underline{\boldsymbol{\mu}}$	Lagrangian multipliers related to power inequalities
$\overline{\boldsymbol{q}_g}$	Upper limits for reactive power of DERs
ρ	Parameter in regularized function
$\underline{\boldsymbol{q}_g}$	Lower limits for reactive power of DERs
c_i	Non-negative coefficient for regulating tap ratio of the i^{th} OLTC
k	Time instant
N	Number of load buses
N_c	Control horizon
n_i	Tap ratio of the i^{th} OLTC
n_i^{max}	Upper tap ratio limit of the i^{th} OLTC
n_i^{min}	Lower tap ratio limit of the i^{th} OLTC
N_p	Prediction horizon
N_t	Number of OLTCs
p_j	Net active power injection at bus j
P_{ij}	Active power from bus i to bus j
q_j	Net reactive power injection at bus j
q_j^g	Reactive power generated by DER at bus j
q_j^l	Load reactive power consumption at bus j
Q_{ij}	Reactive power from bus i to bus j
r_{ij}	Resistance of line segment (i,j)
$s_{\varepsilon j}$, $s_{\delta j}$	Slack variables associated with bus j in the first

This work was fully supported by the Research Grants Council of the Hong Kong Special Administrative Region under the Theme-based Research Scheme through Project No. T23-701/14-N.

Z. Tang is with the Department of Electrical and Computer Engineering, University of Waterloo, Canada (email: zhiyuan.tang@uwaterloo.ca).

T. Liu is with the Department of Electrical and Electronic Engineering, The University of Hong Kong, Hong Kong (email: taoliu@eee.hku.hk).

David J. Hill is with the School of Electrical Engineering and Telecommunications, The University of New South Wales (e-mail: david.hill1@unsw.edu.au).

	stage
$s_{\varphi j}$, $s_{\xi j}$	Slack variables associated with bus j in the second stage
v_j	Voltage magnitude at bus j
v_j^{max}	Upper voltage limit of bus j
v_j^{min}	Lower voltage limit of bus j
v_S	Voltage at substation
x_{ij}	Reactance of line segment (i, j)

I. Introduction

Driven by the environmental concerns, modern power distribution networks have been integrating more and more distributed renewable energy sources, such as photovoltaic (PV) panels. However, due to the high R/X ratio of distribution lines, the high variability of renewables' power generation and abrupt load change due to electric vehicle charging can result in fast voltage fluctuations which may further lead to unexpected voltage violations (over/under voltages). These voltage issues cannot be fully handled by the slow control actions of traditional voltage regulators such as on-load tap changers (OLTCs) and switched capacitors [1]–[4].

In order to solve these voltage issues, distributed energy resources (DERs) have been designed to provide fast and flexible reactive power support [5], [6]. In order to coordinate numerous DERs in a distribution network, different control methods have been proposed for voltage regulation. According to the control architecture, these methods can be categorized as: decentralized, centralized, and distributed methods.

The simplest approach which is also the mostly widely used one is decentralized control. This decentralized method designs voltage control strategies only relying on local voltage information (e.g., [1], [2], [7]–[9]). However, it fails to achieve an optimal control due to the lack of information exchange, and in particular, the control performance degrades when the control limits of DERs are reached [2], [8]. Another approach is centralized control which formulates the voltage control problem as an optimal reactive power flow one, and is solved by using the full system information available (e.g., [3], [4], [10]). However, the centralized approach fails to account for the limited and low-quality communication infrastructure currently employed in distribution networks [5], and lacks scalability to incorporate the increasing number of DERs in active distribution networks.

To strike a balance between decentralized and centralized control, distributed voltage control strategies have been proposed by leveraging information exchange among neighboring nodes (see [6], [11], [12] for examples). However, all these works describe offline algorithms where each control device has to wait for the updated control signal until the iteration of the algorithm converges to obtain a solution for the next step. This may not adapt to fast time-varying operating conditions caused by variable renewable power. To solve this issue, online algorithms need to be developed where the control signal of each device is adjusted by the algorithm at each iteration based on the measured data [5]. Although there are a few distributed online algorithms proposed for voltage regulation (e.g., [5], [13]), they only utilize the DERs as the voltage regulators and do not consider the coordination of DERs with traditional voltage regulators such as OLTCs. It is shown in [11] that an optimal control scheme of DERs may have negative impacts on the existing OLTCs. Thus, the coordination between different types of devices is required. A two-level control architecture has been proposed in [14] to coordinate different types of devices for voltage regulation of sub-transmission networks, but it cannot be used here because the time required to solve its control problem may not be consistent with the fast time-varying operation conditions in distribution networks.

To address these issues, in this paper, we develop a novel distributed coordinated voltage control framework to handle the unexpected voltage violations in active distribution networks. The proposed control framework coordinates OLTCs on slow-timescale (first stage) and reactive power of DERs on fast-timescale (second stage), both in distributed manners. These two stages are designed in a complementary way to incorporate OLTCs and DERs. Particularly, in the first stage, based on predictions of load variations and renewable outputs, OLTCs are coordinated through a distributed multitime-step control (DMC) framework to handle potential voltage violations. However, due to the prediction error and control inaccuracy of OLTCs, the voltage violations may not be fully mitigated. In this case, a novel online distributed algorithm is proposed to coordinate the reactive powers of DERs to bring the violated voltages within their allowable ranges quickly, which forms the second stage. The main contributions of this paper are listed below:

1) Based on different control characteristics, the proposed control framework can coordinate both the discrete slow voltage controllers (i.e., OLTCs) and the continuous fast voltage controllers (i.e., DERs) in a complementary manner via a hierarchical structure. In particular, the first stage acts as a preventive primary controller to handle the potential voltage violations in advance, whereas the second stage acts as a corrective supplementary controller to support voltage control in the first stage.
2) In the first stage, in order to effectively calculate the control schedules of OLTCs in a distributed manner, we firstly convert the original mixed-integer nonlinear problem (MINLP) to a convex one by using linearized DistFlow equations, relaxing discrete decision variables to continous ones, and approximating non-convex voltage relationship of OLTC with a convex one. Then, based on the alternating direction method of multipliers (ADMM) algorithm, a distributed algorithm is proposed to solve the relaxed problem by partitioning the whole distribution network into several control areas where two neighboring control areas are interconnected through an OLTC.
3) In the second stage, by adopting dual decomposition and accelerated gradient projected techniques, a fast online distributed algorithm is proposed for DERs, which considers the most up-to-date system conditions by incorporating voltage measurements at each iteration.

Although there are several centralized approaches proposed in [3], [4], [15], [16] to coordinate both OLTCs and DERs

for voltage regulation in distribution networks, compared with these works, our distributed approach has the following three advantages. The first advantage is the improved applicability. The methods proposed in [3], [4], [15], [16] are only suitable for the case where there is one OLTC located at a substation in the network, whereas our approach can handle the case where there are several OLTCs dispersed at different locations. The second advantage comes from the improved control accuracy. In control schemes proposed in [3], [4], [15], [16], for the convenience of algorithm development, approximate system models are employed, e.g., static voltage sensitivities in [3], [4] and linearized DistFlow model in [15]. However, the control inaccuracy introduced by these approximations are not handled in these works. While in our approach, although approximate models are employed for algorithm design in the first stage, an online control algorithm is designed in the second stage to correct these errors. The advantage of this is demonstrated through comparison with a centralized approach in Scenario 2 of Section IV. The third advantage is the improved reliability. On the one hand, for the centralized approaches in [3], [4], [15], [16], each controller needs to communicate with the the centralized control center (CCC). If the system is large, long-distance communication is unavoidable. While in our approach, this issue can be avoided since each controller only needs to communicate with its local control center (LCC) (first stage) or its neighboring buses (second stage). On the other hand, for a centralized approach, if a communication failure occurs between a controller and CCC, the whole control scheme fails to work. While in our approach, owing to the distributed and hierarchical design, 1) in the first stage, even if the control scheme of a local control area fails due to communication failures, the remaining local control areas can still work based on local measurements, and 2) even if the whole first control stage fails to work, the second stage can still handle the remaining voltage problems.

The rest of the paper is organized as follows. Section II introduces the distribution network model to be studied. The proposed distributed control framework is explicitly presented in Section III. Various case studies based on modified IEEE 34-bus and 123-bus test feeders are given in Section IV. Conclusions are presented in Section V.

II. Network Description

In this section, we introduce the distribution network model that will be employed to develop the proposed coordinated voltage control framework.

Consider a connected radial distribution network with N_b load buses and N_t OLTCs. The substation is modeled as an infinite bus with its voltage magnitude fixed and equal to 1, i.e., $v_S = 1$ p.u.. A radial feeder illustration is shown in Fig. 1 and a typical example is given in Fig. 5.

For the i^{th} OLTC located on the distribution line segment (s_i, f_i) shown in Fig. 1, its standard (conventional) model is given in Fig. 2(a). This model has been widely employed in the literature for voltage control scheme design (see [17]–[19] for examples). To better formulate the branch flow later, we assume that the secondary side of OLTC s_i is the closest side

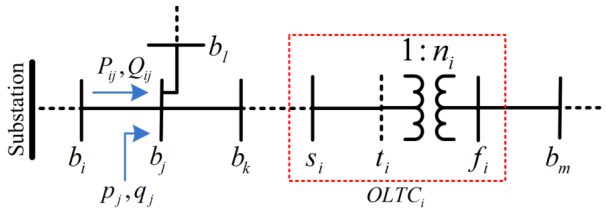

Figure 1: A radial feeder illustration

to the feeder head. The OLTC model is represented by an impedance $z_{t_i} = r_{t_i} + jx_{t_i}$ with an ideal transformer directly connected to the primary-side bus f_i and introduced virtual secondary-side bus t_i such that $v_{f_i} = n_i v_{t_i}$ [17], [18], where the resistance, i.e. the core loss r_{t_i} is typically ignored in distribution systems [19]. The tap ratio n_i is a discrete variable and takes on $2\tilde{m}+1$ possible values $\{\tilde{n}_{-\tilde{m}}, \ldots, \tilde{n}_0, \ldots, \tilde{n}_{\tilde{m}}\}$ that are uniformly distributed within the range $[n^{min}, n^{max}]$ with $n^{min} = \tilde{n}_{-\tilde{m}}$ and $n^{max} = \tilde{n}_{\tilde{m}}$. For instance, with $\tilde{m} = 10$ and $[n^{min}, n^{max}] = [0.9, 1.1]$ p.u., the tap can move up and down 10 positions from the nominal tap ratio $\tilde{n}_0 = 1$ p.u. with each step corresponding to 0.01 p.u.. Fig. 2(b) shows the π equivalent model of the standard model in Fig. 2(a) where the ideal transformer is removed. The relationship of parameters in Fig. 2(a) and Fig. 2(b) is: $z_{\pi_i} = n_i z_{t_i}$, $y_{\pi 1_i} = (n_i - 1)/(n_i z_{t_i})$, and $y_{\pi 2_i} = (1 - n_i)/(n_i^2 z_{t_i})$.

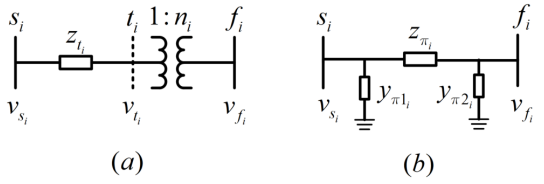

Figure 2: OLTC model. (a) Classical OLTC model. (b) Equivalent OLTC model

Let $\mathcal{T} = \{1, \ldots, N_t\}$ be the set of OLTCs. The set of virtual secondary-side buses introduced in the OLTC model shown in Fig. 2(a) is defined as $\mathcal{N}_t = \{t_1, \ldots, t_{N_t}\}$. The set of buses incident to the primary-side and secondary-side of a OLTC are defined as $\mathcal{N}_f = \{f_1, \ldots, f_{N_t}\}$ and $\mathcal{N}_s = \{s_1, \ldots, s_{N_t}\}$, respectively. The remaining system buses are represented as the set $\mathcal{N}_b = \{b_0, b_1, \ldots, b_{N_b}\}$. Then, the set of buses in the augmented network created with the virtual buses is defined as $\mathcal{N} = \mathcal{N}_t \cup \mathcal{N}_f \cup \mathcal{N}_s \cup \mathcal{N}_b$ with $|\mathcal{N}| = N = N_b + 3N_t + 1$ and the line segment set is defined as $\mathcal{E} := \{(i,j)\} \subseteq \mathcal{N} \times \mathcal{N}$ with $|\mathcal{E}| = N_b + 3N_t$. For each bus i, $i \in \mathcal{N}_b$, we assume that there is one DER with electronic interface (e.g. PV) that can regulate its active and reactive power outputs respectively.

Considering the OLTC model in Fig. 2(a), based on the type of branches, the power flow equations of the network are formulated as follows:

1) Branch with an ideal transformer: The power transferred across the line segment (t_i, f_i), $i \in \mathcal{T}$ (i.e., ideal transformer) in Fig. 1 remains the same but the tap ratio n_i is

captured by the voltage relationship, i.e.,

$$P_{t_i f_i} = P_{f_i b_m},\ Q_{t_i f_i} = Q_{f_i b_m},\ v_{f_i} = n_i v_{t_i}. \tag{1}$$

Here, bus b_m is the descendant neighbor of bus f_i.

2) Branch without an ideal transformer: The DistFlow equations proposed in [20] are employed to model the power flow for each branch $(i,j) \in \mathcal{E}$, $i \in \mathcal{N}\backslash\mathcal{N}_t$ in Fig. 1 without an ideal transformer:

$$P_{ij} - \sum_{k\in\mathcal{N}_j^d} P_{jk} = -p_j + r_{ij}\frac{P_{ij}^2 + Q_{ij}^2}{v_i^2} \tag{2a}$$

$$Q_{ij} - \sum_{k\in\mathcal{N}_j^d} Q_{jk} = -q_j + x_{ij}\frac{P_{ij}^2 + Q_{ij}^2}{v_i^2} \tag{2b}$$

$$v_i^2 - v_j^2 = 2(r_{ij}P_{ij} + x_{ij}Q_{ij}) - (r_{ij}^2 + x_{ij}^2)\frac{P_{ij}^2 + Q_{ij}^2}{v_i^2}. \tag{2c}$$

where v_j, p_j, and q_j denote the voltage magnitude, net active and reactive power injection of bus j, respectively. Further, note: 1) $q_j = q_j^g - q_j^l$ with q_j^g defines the reactive power generated by DER of bus j and q_j^l defines the load reactive power consumption at bus j; 2) P_{ij}, Q_{ij} are the active and reactive power from bus i to bus j, respectively; 3) r_{ij} and x_{ij} are the resistance and reactance of line segment (i,j), respectively; and 4) the nonlinear term $(P_{ij}^2 + Q_{ij}^2)/v_i^2$ represents the squared line current magnitude that is associated with the loss term in (2a)-(2c). For convenience, we use set $\mathcal{N}_j^d$ to denote all bus j's descendant neighbors.

III. Proposed Control Strategy

In this section, an overview of the proposed control framework is firstly given to show the main ideas. Then, the details of each control stage will be presented.

A. Overview

Voltage violations (over/under voltages) are inevitably caused by the time-varying generation of renewable power. To effectively handle these voltage violations, in this work, a coordinated voltage control framework is proposed by coordinating both OLTCs and reactive power of DERs in a distributed manner. The proposed control framework consists of two stages that are designed in a complementary manner. In the first stage, with the help of short-term predictions of load profile and renewable generation, the OLTCs are coordinated on a slow-timescale to handle the potential voltage violations. However, due to the prediction error and control inaccuracy of OLTCs, the voltage violations may not be fully mitigated. Once an unmanageable voltage violation is detected, the reactive power of DERs will be coordinated immediately to bring the voltages back to their allowable limits, which forms the second control stage.

B. The first stage

In this stage, a DMC framework is proposed to handle the potential voltage violations for OLTCs using of model predictive control (MPC). The principle of DMC is briefly described as follows. At each time instant k, based on the current voltage measurements, the explicit system model (1) and (2) described in Section II, and the short-term predictions of load profile and renewable generation, the future voltages (from k to $k+N_p$) with all allowable control sequences (from k to $k+N_c$ with $N_c = N_p$) are predicted. According to the predicted voltage behavior and a selected cost function, the performance of each candidate control sequence is evaluated by solving a multitime-step constrained optimization problem in a distributed manner, and only the first element of the optimal control sequence is implemented during the current time interval. The whole process is repeated at the next time instant $k+1$. Here, the control process is different from standard MPC because there is no differential equation in the system model (1) and (2) and the control horizon N_c must equal to the prediction horizon N_p.

In the proposed DMC framework, the multitime-step constrained optimization problem used for evaluating candidate control sequences of OLTCs is described as follows. It aims to minimize the number of control actions of OLTCs while satisfying the system model introduced in Section II, control limits, and voltage limits (to avoid voltage violations). The decision variables are tap ratios of N_t OLTCs, i.e., $\boldsymbol{n} = [n_1, \ldots, n_{N_t}]^T$. Here, the superscript 'T' denotes the transpose of a vector or matrix. The control problem is formulated as:

$$\min \sum_{j=0}^{N_c} \frac{1}{2}\left(||\Delta\boldsymbol{n}(k+j)||_{\boldsymbol{C}}^2 + ||\boldsymbol{\varepsilon}||_{\boldsymbol{\Upsilon}}^2 + ||\boldsymbol{\delta}||_{\boldsymbol{\Delta}}^2\right) \tag{3a}$$

subject to

$$\text{system equations (1) and (2)} \tag{3b}$$

$$\boldsymbol{n}^{min} \le \boldsymbol{n}(k+j) + \Delta\boldsymbol{n}(k+j) \le \boldsymbol{n}^{max}, j = 0, \ldots, N_c \tag{3c}$$

$$-\boldsymbol{\varepsilon} + \boldsymbol{v}^{min} \le \boldsymbol{v}(k+j) \le \boldsymbol{v}^{max} + \boldsymbol{\delta}, j = 0, 1, \ldots, N_p \tag{3d}$$

where $||\Delta\boldsymbol{n}||_{\boldsymbol{C}}^2 = \Delta\boldsymbol{n}^T\boldsymbol{C}\Delta\boldsymbol{n}$ and the diagonal matrix $\boldsymbol{C} = \text{diag}(\boldsymbol{c})$ with diagonal elements $\boldsymbol{c} = [c_1, \ldots, c_{N_t}]^T$ giving different weights to different OLTCs. The vector $\boldsymbol{v} = [v_1, \ldots, v_N]^T$ defines the set of all bus voltage magnitudes. The vectors $\boldsymbol{v}^{max} = [v_1^{max}, \ldots, v_N^{max}]^T$ and $\boldsymbol{v}^{min} = [v_1^{min}, \ldots, v_N^{min}]^T$ are the sets of upper and lower limits on bus voltages. The vectors $\boldsymbol{n}^{max} = [n_1^{max}, \ldots, n_{N_t}^{max}]^T$ and $\boldsymbol{n}^{min} = [n_1^{min}, \ldots, n_{N_t}^{min}]^T$ are the sets of upper and lower limits on tap ratios. The vectors $\boldsymbol{\varepsilon} = [\varepsilon_1, \ldots, \varepsilon_N]^T$ and $\boldsymbol{\delta} = [\delta_1, \ldots, \delta_N]^T$ with non-negative entries are slack variables introduced in (3d) to relax the hard voltage constraints to soft ones. In this way, the problem (3) will be feasible even if there is no sufficient control resources [3]. The slack variables $\boldsymbol{\varepsilon}$ and $\boldsymbol{\delta}$ are heavily penalized in the cost function by using the diagonal weight matrices $\boldsymbol{\Upsilon} = \text{diag}(\boldsymbol{s}_\varepsilon)$ and $\boldsymbol{\Delta} = \text{diag}(\boldsymbol{s}_\delta)$ with large diagonal elements $\boldsymbol{s}_\varepsilon = [s_{\varepsilon 1}, \ldots, s_{\varepsilon N}]^T$ and $\boldsymbol{s}_\delta = [s_{\delta 1}, \ldots, s_{\delta N}]^T$ [3].

From (3), we can see that the control problem (3) is an MINLP due to the presence of integer variable $\boldsymbol{n}$ and nonconvex nonlinear system equations (1) and (2), which cannot

be solved easily in a distributed manner due to convergence issues, computational complexity, and curse of dimensionality. To handle this, we use the following:

1) relax the discrete variables n_i, $i \in \mathcal{T}$ to continuous variables that take values on the interval $[n_i^{min}, n_i^{max}]$. Once the optimal n_i is obtained, it will be rounded to its closest discrete value.
2) partition the whole distribution network into N_t local control areas CA_i, $i \in \mathcal{T}$, where the primary-side f_i and virtual secondary-side buses t_i of each OLTC located at a boundary between two local control areas (see Fig. 3 for illustration).
3) adopt the linearized DistFlow model in [2] to model the power flow equations (2) for each local control area.
4) approximate the voltage change of primary-side bus of each OLTC Δv_{fi} with $\Delta n_i v_{t_i} + n_i \Delta v_{t_i}$ by ignoring the non-convex term $\Delta n_i \Delta v_{t_i}$.

By doing so, the original MINLP (3) can be cast as a quadratic program (QP) that can be solved in a distributed manner. The formulation is described below.

Firstly, based on the abovementioned network decomposition method, we decompose the bus set $\mathcal{N}$ into N_t distinct local bus sets $\mathcal{N}_i = \{b_0^i, b_1^i, \ldots, b_{N_i}^i\}$, $i \in \mathcal{T}$ with $|\mathcal{N}_i| = N_i + 1$ and $\sum_{i\in\mathcal{T}} |\mathcal{N}_i| = |\mathcal{N}|$. We call the area that contains the bus set $\mathcal{N}_i$ as the i^{th} control area and denote it as CA_i. We also define the line segment set of CA_i, $i \in \mathcal{T}$ as $\mathcal{E}_i \coloneqq \{(i,j)\} \subseteq \mathcal{N}_i \times \mathcal{N}_i$. Fig. 3 shows the decomposition method.

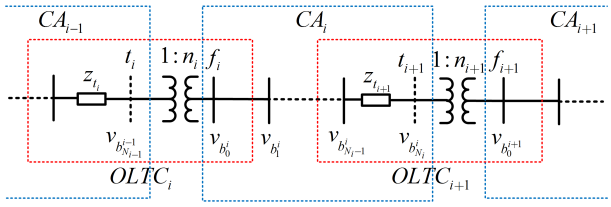

Figure 3: The decomposition procedure

On the basis of the above definitions, for each control area CA_i, $i \in \mathcal{T}$, the primary-side bus of the i^{th} OLTC is regarded as a local feeder bus, and the remaining buses in this area are regarded as the non-feeder buses. Then, based on (2), the linearized DistFlow equations (4) can be established by assuming that 1) the loss is negligible compared to line flow, and 2) the voltage profile is relatively flat, i.e., $v_j^2 - v_k^2 \approx 2(v_j - v_k)$, $(j,k) \in \mathcal{E}_i$ [2], [9]:

$$\boldsymbol{v}_i = \boldsymbol{R}_i \boldsymbol{p}_i + \boldsymbol{X}_i \boldsymbol{q}_i + v_{b_0^i} \mathbf{1}_{N_i} \tag{4}$$

where $v_{b_0^i} = n_i v_{t_i}$ with $v_{t_i} = v_{b_{N_{i-1}}^{i-1}}$, which describes the voltage relationship of OLTC given in (1). The vectors $\boldsymbol{v}_i = [v_{b_1^i}, \ldots, v_{b_{N_i}^i}]^T$, $\boldsymbol{p}_i = [p_{b_1^i}, \ldots, p_{b_{N_i}^i}]^T$, and $\boldsymbol{q}_i = [q_{b_1^i}, \ldots, q_{b_{N_i}^i}]^T$ are the bus voltages, active power injections, and reactive power injections, respectively. Vector $\mathbf{1}_{N_i} \in R^{N_i}$ is the all-ones vector. The matrices $\boldsymbol{R}_i = \boldsymbol{F}_i \text{diag}(\boldsymbol{r}_i) \boldsymbol{F}_i^T$ and $\boldsymbol{X}_i = \boldsymbol{F}_i \text{diag}(\boldsymbol{x}_i) \boldsymbol{F}_i^T$ with $\boldsymbol{r}_i = [r_{b_{jk}^i}] \in R^{N_i}$, $(j,k) \in \mathcal{E}_i$ and $\boldsymbol{x}_i = [x_{b_{jk}^i}] \in R^{N_i}$, $(j,k) \in \mathcal{E}_i$ are the resistance and reactance of line segment, respectively. The matrix $\boldsymbol{F}_i = -\boldsymbol{Z}_i^{-1}$ where $\boldsymbol{Z}_i$ is the reduced branch-bus incidence matrix [9]. It is worth mentioning that the accuracy of the linearized DistFlow model (4) has been corroborated by recent works [9] and [12].

Then, based on (4), the bus voltage changes in the control area CA_i, $i \in \mathcal{T}$ can be estimated by:

$$\begin{aligned} \Delta \boldsymbol{v}_i =& \boldsymbol{R}_i \Delta \boldsymbol{p}_i + \boldsymbol{X}_i \Delta \boldsymbol{q}_i + \Delta v_{b_0^i} \mathbf{1}_{N_i} \\ =& \boldsymbol{R}_i \Delta \boldsymbol{p}_i + \boldsymbol{X}_i \Delta \boldsymbol{q}_i + (\Delta n_i v_{t_i} + n_i \Delta v_{t_i}) \mathbf{1}_{N_i} \end{aligned} \tag{5}$$

where $\Delta v_{b_i^0} = \Delta n_i v_{t_i} + n_i \Delta v_{t_i} + \Delta n_i \Delta v_{t_i}$ is approximated as $\Delta n_i v_{t_i} + n_i \Delta v_{t_i}$ by ignoring the negligible quadratic term $\Delta n_i \Delta v_{t_i}$. Note that the accuracy of this approximation has been verified by the case study (see Section IV for details).

Finally, based on (5), the original MINLP (3) is relaxed to the following new QP problem:

$$\min \sum_{i\in\mathcal{T}} \left\{ \sum_{j=0}^{N_c} \frac{1}{2} \left(c_i \Delta n_i^2 (k+j) + ||\boldsymbol{\varepsilon}_i||^2_{\boldsymbol{\Upsilon}_i} + ||\boldsymbol{\delta}_i||^2_{\boldsymbol{\Delta}_i} \right) \right\} \tag{6a}$$

subject to (5) and for $j = 0, 1, \ldots, N_p$:

$$n_i^{min} \le n_i(k+j) + \Delta n_i(k+j) \le n_i^{max}, \forall i \in \mathcal{T} \tag{6b}$$

$$-\boldsymbol{\varepsilon}_i + \boldsymbol{v}_i^{min} \le \boldsymbol{v}_i(k+j) \le \boldsymbol{v}_i^{max} + \boldsymbol{\delta}_i, \forall i \in \mathcal{T} \tag{6c}$$

$$\boldsymbol{v}_i(k+j) = \boldsymbol{v}_i^{mea}(k) + \Delta \boldsymbol{v}_i(k+j), \forall i \in \mathcal{T}. \tag{6d}$$

Here $\boldsymbol{\varepsilon}_i = [\varepsilon_{b_1^i}, \ldots, \varepsilon_{b_{N_i}^i}]^T$ and $\boldsymbol{\delta}_i = [\delta_{b_1^i}, \ldots, \delta_{b_{N_i}^i}]^T$ are the slack variable vectors of the i^{th} control area CA_i, which are the corresponding part of the slack variable vectors $\boldsymbol{\varepsilon}$ and $\boldsymbol{\delta}$ in (3), respectively. The matrices $\boldsymbol{\Upsilon}_i$ and $\boldsymbol{\Delta}_i$ are diagonal weight matrices of the i^{th} control area CA_i, whose diagonal elements are the corresponding part of the weighting vectors $\boldsymbol{s}_\varepsilon$ and $\boldsymbol{s}_\delta$ in (3), respectively. The vector $\boldsymbol{v}_i^{mea}(k)$ in (6d) is the real-time voltage measurement that is updated by the controller at each time instant k. The vector $\boldsymbol{v}_i(k+j)$ in (6d) is the predicted bus voltage magnitude that is calculated based on the current voltage measurement $\boldsymbol{v}_i^{mea}(k)$ and the predicted voltage variation $\Delta \boldsymbol{v}_i(k+j)$ with respect to control variables, predicted load profile, and renewable generation whose relationship is described by (5).

It should be noted that problem (6) is convex and separable based on the partitioned control areas. Inspired by these properties, we propose to use the ADMM [21] to solve the problem in a distributed way. ADMM has been proven to be a powerful and efficient distributed optimization method [5], [12], [21], which iteratively minimizes the augmented Lagrangian over three types of variable, i.e., the decision variable, the auxiliary variable, and the dual variable until convergence. During each iteration of ADMM, each type of variable is updated while fixing the others [21]. The general discussion of ADMM can be found in [21].

To solve problem (6) by using ADMM, we assign two auxiliary variables $\Delta v_{t_i^i}$ and $\Delta v_{t_{i+1}^i}$ to each control area CA_i, $i \in \mathcal{T}$ that are used to enforce the equality boundary conditions on bus voltages between neighboring areas, i.e., $\Delta v_{t_i^{i-1}} = \Delta v_{t_i^i} = \Delta v_{t_i}$ and $\Delta v_{t_{i+1}^i} = \Delta v_{t_{i+1}^{i+1}} = \Delta v_{t_{i+1}}$ (see Fig. 3 for illustration). Given the above auxiliary variables, the ADMM-based method is designed to solve problem (6) in an

iterative and distributed manner. The details of τ^{th} iteration are given as below.

1) Decision variables update: For each control area CA_i, $i \in \mathcal{T}$, the decision variable $\Delta n_i(k+j)(\tau)$, $j = 0, 1, \ldots, N_c$ and two auxiliary variables $\Delta v_{t_i^i}(\tau)$ and $\Delta v_{t_{i+1}^i}(\tau)$ are updated by solving the following local QP problem through local augmented Lagrangian function $\mathcal{L}_i$:

$$\min \mathcal{L}_i \tag{7a}$$

subject to

$$(5), (6b), (6c), \text{ and } (6d). \tag{7b}$$

Here, $\mathcal{L}_i$ is defined as

$$\begin{aligned}\mathcal{L}_i = &\sum_{j=0}^{N_c} \frac{1}{2}\left(c_i \Delta n_i^2(k+j) + ||\boldsymbol{\varepsilon}_i||^2_{\boldsymbol{\Upsilon}_i} + ||\boldsymbol{\delta}_i||^2_{\boldsymbol{\Delta}_i}\right) \\ &+ \frac{\rho}{2}(\Delta v_{t_i^i} - \Delta v_{t_i})^2 + \frac{\rho}{2}(\Delta v_{t_{i+1}^i} - \Delta v_{t_{i+1}})^2 \\ &+ \lambda_i^i(\Delta v_{t_i^i} - \Delta v_{t_i}) + \lambda_{i+1}^i(\Delta v_{t_{i+1}^i} - \Delta v_{t_{i+1}})\end{aligned} \tag{8}$$

where the local equality boundary conditions are regularized by the additional quadratic terms with coefficient ρ. The symbols λ_i^i and λ_{i+1}^i are dual variables related to the boundary conditions.

2) Auxiliary variables update: This step updates the global variables Δv_{t_i} and $\Delta v_{t_{i+1}}$ that are shared with neighboring control areas. The update process is given as

$$\Delta v_{t_i}(\tau) = \frac{1}{2}\left(\Delta v_{t_i^{i-1}}(\tau) + \Delta v_{t_i^i}(\tau)\right) \tag{9a}$$

$$\Delta v_{t_{i+1}}(\tau) = \frac{1}{2}\left(\Delta v_{t_{i+1}^i}(\tau) + \Delta v_{t_{i+1}^{i+1}}(\tau)\right) \tag{9b}$$

where the communication between neighboring control areas is required.

3) Dual variables update: The dual variables are updated locally by the following process

$$\lambda_i^i(\tau) = \lambda_i^i(\tau-1) + \rho\left(\Delta v_{t_i^i}(\tau) - \Delta v_{t_i}(\tau)\right) \tag{10a}$$

$$\lambda_{i+1}^i(\tau) = \lambda_{i+1}^i(\tau-1) + \rho\left(\Delta v_{t_{i+1}^i}(\tau) - \Delta v_{t_{i+1}}(\tau)\right). \tag{10b}$$

Based on the principle of DMC and abovementioned ADMM-based method, the control framework is summarized as follows:

1) At time instant k, each control area CA_i, $i \in \mathcal{T}$ gathers information of local current voltage measurements, predicted load profile and renewable generation (from k to $k+N_p$).
2) Based on the information obtained in step 1, each control area CA_i, $i \in \mathcal{T}$ calculates its own optimal control sequence of OLTC by solving the control problem (6) through communication with its neighboring areas via the proposed ADMM-based method.
3) Each control area CA_i, $i \in \mathcal{T}$ applies the first element of the optimal control sequence obtained in step 2 during the current time interval $[k, k+1]$. Proceed to next time instant $k+1$, go to step 1.

C. The second stage

Although OLTCs are utilized in the first stage to handle the potential voltage violations based on predicted load profile and renewable generation, due to the discrete control nature of OLTCs, prediction errors, and linearization of system equations introduced in (6), the voltage violations may not be fully avoided. To handle this problem, a distributed online voltage control framework is designed in this stage by coordinating the reactive power of DERs.

The control problem considered here aims to minimize the cost of reactive power supply while satisfying the voltage and control limits. This can be formulated by the following optimization problem:

$$\min \frac{1}{2}\left(||\boldsymbol{q}^g||^2_{\boldsymbol{D}} + ||\boldsymbol{\varphi}||^2_{\boldsymbol{\Phi}} + ||\boldsymbol{\xi}||^2_{\boldsymbol{\Xi}}\right) \tag{11a}$$

subject to

$$-\boldsymbol{\varphi} + \boldsymbol{v}^{min} \le \boldsymbol{v} \le \boldsymbol{v}^{max} + \boldsymbol{\xi} \tag{11b}$$

$$\underline{\boldsymbol{q}^g} \le \boldsymbol{q}^g \le \overline{\boldsymbol{q}^g} \tag{11c}$$

where $\boldsymbol{q}^g = [q_1^g, \ldots, q_{N_b}^g]^T$ defines the reactive power generated by DERs and $\boldsymbol{D}$ is the weight matrix that is positive definite. Similar to the first stage, in order to make the problem feasible, the non-negative vectors $\boldsymbol{\varphi} = [\varphi_1, \ldots, \varphi_{N_b}]^T$ and $\boldsymbol{\xi} = [\xi_1, \ldots, \xi_{N_b}]^T$ are slack variables introduced to convert the hard voltage constraints to soft ones. To regulate the bus voltages within the allowable range $[\boldsymbol{v}^{min}, \boldsymbol{v}^{max}]$ whenever possible, these slack variables are heavily penalized in the cost function by using the diagonal weight matrices $\boldsymbol{\Phi} = \text{diag}(\boldsymbol{s}_\varphi)$ with $\boldsymbol{s}_\varphi = [s_{\varphi 1}, \ldots, s_{\varphi N_b}]^T$ and $\boldsymbol{\Xi} = \text{diag}(\boldsymbol{s}_\xi)$ with $\boldsymbol{s}_\xi = [s_{\xi 1}, \ldots, s_{\xi N_b}]^T$. The vectors $\underline{\boldsymbol{q}^g} = [\underline{\boldsymbol{q}_1^g}, \ldots, \underline{\boldsymbol{q}_{N_b}^g}]^T$ and $\overline{\boldsymbol{q}^g} = [\overline{\boldsymbol{q}_1^g}, \ldots, \overline{\boldsymbol{q}_{N_b}^g}]^T$ define the lower and upper limits for reactive power of DERs.

In order to apply a distributed online control strategy, we adopt the dual ascent algorithm in [22] to solve (11). Specifically, we approximate the primal optimizer by using the linearized DistFlow model to derive distributed update steps for dual ascent algorithm, and apply the accelerated gradient projected technique [23] in the dual update steps to improve the convergence speed of dual ascent algorithm.

The Lagrangian of (11) is

$$\begin{aligned}\mathcal{L} = &\frac{1}{2}\left(||\boldsymbol{q}^g||^2_{\boldsymbol{D}} + ||\boldsymbol{\varphi}||^2_{\boldsymbol{\Phi}} + ||\boldsymbol{\xi}||^2_{\boldsymbol{\Xi}}\right) \\ &+ \underline{\boldsymbol{\lambda}}^T(-\boldsymbol{v} + \boldsymbol{v}^{min} - \boldsymbol{\varphi}) + \overline{\boldsymbol{\lambda}}^T(\boldsymbol{v} - \boldsymbol{v}^{max} - \boldsymbol{\xi}) \\ &+ \underline{\boldsymbol{\mu}}^T(-\boldsymbol{q}^g + \underline{\boldsymbol{q}^g}) + \overline{\boldsymbol{\mu}}^T(\boldsymbol{q}^g - \overline{\boldsymbol{q}^g})\end{aligned} \tag{12}$$

where vectors $\underline{\boldsymbol{\lambda}}$, $\overline{\boldsymbol{\lambda}}$, $\underline{\boldsymbol{\mu}}$, and $\overline{\boldsymbol{\mu}}$ are the Lagrangian multipliers (dual variables) associated with the inequality constraints. For convenience, we define $\boldsymbol{\phi}$ as $\boldsymbol{\phi} = [\underline{\boldsymbol{\lambda}}^T, \overline{\boldsymbol{\lambda}}^T, \underline{\boldsymbol{\mu}}^T, \overline{\boldsymbol{\mu}}^T]^T$. Based on dual ascent algorithm, the solutions of (11) can be calculated via the following iterative execution [13], [23]:

1) Dual variable update: dual gradient ascent step on the dual variables

$$\begin{aligned}
\underline{\boldsymbol{\lambda}}(\tau+1) &= \left[\underline{\boldsymbol{\lambda}}(\tau)+\gamma\frac{\partial\mathcal{L}(\boldsymbol{q}^g(\tau),\boldsymbol{\varphi}(\tau),\boldsymbol{\xi}(\tau),\boldsymbol{\phi}(\tau))}{\partial\underline{\boldsymbol{\lambda}}(\tau)}\right]_+\\
\overline{\boldsymbol{\lambda}}(\tau+1) &= \left[\overline{\boldsymbol{\lambda}}(\tau)+\gamma\frac{\partial\mathcal{L}(\boldsymbol{q}^g(\tau),\boldsymbol{\varphi}(\tau),\boldsymbol{\xi}(\tau),\boldsymbol{\phi}(\tau))}{\partial\overline{\boldsymbol{\lambda}}(\tau)}\right]_+\\
\underline{\boldsymbol{\mu}}(\tau+1) &= \left[\underline{\boldsymbol{\mu}}(\tau)+\gamma\frac{\partial\mathcal{L}(\boldsymbol{q}^g(\tau),\boldsymbol{\varphi}(\tau),\boldsymbol{\xi}(\tau),\boldsymbol{\phi}(\tau))}{\partial\underline{\boldsymbol{\mu}}(\tau)}\right]_+\\
\overline{\boldsymbol{\mu}}(\tau+1) &= \left[\overline{\boldsymbol{\mu}}(\tau)+\gamma\frac{\partial\mathcal{L}(\boldsymbol{q}^g(\tau),\boldsymbol{\varphi}(\tau),\boldsymbol{\xi}(\tau),\boldsymbol{\phi}(\tau))}{\partial\overline{\boldsymbol{\mu}}(\tau)}\right]_+
\end{aligned} \tag{13}$$

where the operator $[\cdot]_+$ defines the projection on the positive orthant and γ is a suitable positive constant.

2) Primal variable update: minimization of the Lagrangian with respect to the primal variables

$$\begin{aligned}
\boldsymbol{\varphi}(\tau+1) &= \arg\min_{\boldsymbol{\varphi}}\mathcal{L}(\boldsymbol{q}^g,\boldsymbol{\varphi},\boldsymbol{\xi},\boldsymbol{\phi}(\tau+1))\\
\boldsymbol{\xi}(\tau+1) &= \arg\min_{\boldsymbol{\xi}}\mathcal{L}(\boldsymbol{q}^g,\boldsymbol{\varphi},\boldsymbol{\xi},\boldsymbol{\phi}(\tau+1))\\
\boldsymbol{q}^g(\tau+1) &= \arg\min_{\boldsymbol{q}^g}\mathcal{L}(\boldsymbol{q}^g,\boldsymbol{\varphi},\boldsymbol{\xi},\boldsymbol{\phi}(\tau+1)).
\end{aligned} \tag{14}$$

Substituting (12) into (13), we find that the update of dual variables can be easily conducted in a local manner based on the real-time measurements of violations of the voltage and control constraints:

$$\begin{aligned}
\underline{\boldsymbol{\lambda}}(\tau+1) &= \left[\underline{\boldsymbol{\lambda}}(\tau)+\gamma(-\boldsymbol{v}(\tau)+\boldsymbol{v}^{min}-\boldsymbol{\varphi}(\tau))\right]_+\\
\overline{\boldsymbol{\lambda}}(\tau+1) &= \left[\overline{\boldsymbol{\lambda}}(\tau)+\gamma(\boldsymbol{v}(\tau)-\boldsymbol{v}^{max}+\boldsymbol{\xi}(\tau))\right]_+\\
\underline{\boldsymbol{\mu}}(\tau+1) &= \left[\underline{\boldsymbol{\mu}}(\tau)+\gamma(-\boldsymbol{q}^g(\tau)+\underline{\boldsymbol{q}^g})\right]_+\\
\overline{\boldsymbol{\mu}}(\tau+1) &= \left[\overline{\boldsymbol{\mu}}(\tau)+\gamma(\boldsymbol{q}^g(\tau)-\overline{\boldsymbol{q}^g})\right]_+.
\end{aligned} \tag{15}$$

And substituting (12) into (14), we can see that the update of primal variables $\boldsymbol{\varphi}$ and $\boldsymbol{\xi}$ can also be conducted in a local manner:

$$\begin{aligned}
\boldsymbol{\varphi}(\tau+1) &= \boldsymbol{\Phi}^{-1}\underline{\boldsymbol{\lambda}}(\tau+1)\\
\boldsymbol{\xi}(\tau+1) &= \boldsymbol{\Xi}^{-1}\overline{\boldsymbol{\lambda}}(\tau+1).
\end{aligned} \tag{16}$$

Now the difficulty is to update the primal variable $\boldsymbol{q}^g(\tau+1)$ in a distributed manner.

From $\frac{\partial\mathcal{L}}{\partial\boldsymbol{q}^g}=0$, we obtain

$$\boldsymbol{D}\boldsymbol{q}^g+\left(\frac{\partial\boldsymbol{v}}{\partial\boldsymbol{q}^g}\right)^T(\overline{\boldsymbol{\lambda}}-\underline{\boldsymbol{\lambda}})+(\overline{\boldsymbol{\mu}}-\underline{\boldsymbol{\mu}})=0, \tag{17}$$

which gives

$$\boldsymbol{q}^g=-\boldsymbol{D}^{-1}\left[\left(\frac{\partial\boldsymbol{v}}{\partial\boldsymbol{q}^g}\right)^T(\overline{\boldsymbol{\lambda}}-\underline{\boldsymbol{\lambda}})+(\overline{\boldsymbol{\mu}}-\underline{\boldsymbol{\mu}})\right]. \tag{18}$$

Therefore, the sensitivity matrix $\frac{\partial\boldsymbol{v}}{\partial\boldsymbol{q}^g}$ which contains global information is the key obstacle to design the distributed update process.

In order to obtain a suitable $\frac{\partial\boldsymbol{v}}{\partial\boldsymbol{q}^g}$, we use: 1) the equivalent π model in Fig. 2(b) to represent the ideal transformer introduced for the OLTC model and 2) the linearized DistFlow model instead of the nonlinear power flow equations (2) to describe the relationship between voltages and power injections. Since the two admittance branches $y_{\pi 1_i}$ and $y_{\pi 2_i}$ introduced in the equivalent π model cannot be incorporated in the Linearized DistFlow equations, we replace these two admittance branches with two reactive power loads whose reactive power consumptions are $v_{s_i}^2 y_{\pi 1_i}$ and $v_{f_i}^2 y_{\pi 2_i}$, respectively. In this way, the voltage of the network can be expressed as [2], [9]:

$$\boldsymbol{v}=\boldsymbol{R}\boldsymbol{p}+\boldsymbol{X}(\boldsymbol{q}^g-\boldsymbol{q}^l)+v_S\mathbf{1}_N. \tag{19}$$

where $\boldsymbol{p}=[p_1,\ldots,p_{N_b}]^T$ and $\boldsymbol{q}^l=[q_1^l,\ldots,q_{N_b}^l]^T$. Matrices $\boldsymbol{R}=\boldsymbol{F}\text{diag}(\boldsymbol{r})\boldsymbol{F}^T$ and $\boldsymbol{X}=\boldsymbol{F}\text{diag}(\boldsymbol{x})\boldsymbol{F}^T$ are symmetric and positive-definite [9]. And the sensitivity matrix $\frac{\partial\boldsymbol{v}}{\partial\boldsymbol{q}^g}$ becomes

$$\frac{\partial\boldsymbol{v}}{\partial\boldsymbol{q}^g}=\boldsymbol{X}. \tag{20}$$

Here, the matrix $\boldsymbol{X}$ has an important characteristic that its inverse matrix $\boldsymbol{B}=\boldsymbol{X}^{-1}$ has the same sparsity as that of the nodal admittance matrix, i.e., the matrix $\boldsymbol{B}$ has nonzero entries only in the diagonal position and position $i\in\mathcal{N}_b$, $j\in\mathcal{N}_b$ with $(i,j)\in\mathcal{E}$. Therefore, if we select the weight matrix $\boldsymbol{D}=\boldsymbol{X}$ and substitute (20) into (18), we can get

$$\boldsymbol{q}^g(\tau+1)=-(\overline{\boldsymbol{\lambda}}(\tau+1)-\underline{\boldsymbol{\lambda}}(\tau+1))-\boldsymbol{B}(\overline{\boldsymbol{\mu}}(\tau+1)-\underline{\boldsymbol{\mu}}(\tau+1)) \tag{21}$$

which leads to a distributed computation of the primal variable $\boldsymbol{q}^g$ and therefore a distributed dual-ascent algorithm.

In order to improve the convergence speed of the proposed distributed dual-ascent algorithm, the accelerated gradient projected technique proposed in [23] is employed for the dual variable update process (15), whose advantage has been verified by our previous work [24]:

$$\begin{aligned}
\underline{\boldsymbol{\lambda}}(\tau+1) &= \left[\boldsymbol{\lambda}^{min}(\tau)+\gamma(-\boldsymbol{v}(\tau)+\boldsymbol{v}^{min}-\boldsymbol{\varphi}(\tau))\right]_+\\
\overline{\boldsymbol{\lambda}}(\tau+1) &= \left[\boldsymbol{\lambda}^{max}(\tau)+\gamma(\boldsymbol{v}(\tau)-\boldsymbol{v}^{max}+\boldsymbol{\xi}(\tau))\right]_+\\
\underline{\boldsymbol{\mu}}(\tau+1) &= \left[\boldsymbol{\mu}^{min}(\tau)+\gamma(-\boldsymbol{q}^g(\tau)+\underline{\boldsymbol{q}^g})\right]_+\\
\overline{\boldsymbol{\mu}}(\tau+1) &= \left[\boldsymbol{\mu}^{max}(\tau)+\gamma(\boldsymbol{q}^g(\tau)-\overline{\boldsymbol{q}^g})\right]_+\\
\boldsymbol{\psi}(\tau+1) &= \boldsymbol{\phi}(\tau+1)+\beta(\tau+1)(\boldsymbol{\phi}(\tau+1)-\boldsymbol{\phi}(\tau))
\end{aligned} \tag{22}$$

where $\beta(\tau+1)=\theta(\tau)(1-\theta(\tau))/\left(\theta(\tau)^2+\theta(\tau+1)\right)$ with $\theta(\tau+1)=\frac{\sqrt{\theta(\tau)^4+4\theta(\tau)^2}-\theta(\tau)^2}{2}$. Here $\boldsymbol{\psi}=[\boldsymbol{\lambda}^{min^T},\boldsymbol{\lambda}^{max^T},\boldsymbol{\mu}^{min^T},\boldsymbol{\mu}^{max^T}]^T$ are auxiliary dual vectors, i.e, each bus j has four dual variables ($\underline{\boldsymbol{\lambda}}_j$, $\overline{\boldsymbol{\lambda}}_j$, $\underline{\boldsymbol{\mu}}_j$, $\overline{\boldsymbol{\mu}}_j$) and four auxiliary dual variables ($\boldsymbol{\lambda}_j^{min}$, $\boldsymbol{\lambda}_j^{max}$, $\boldsymbol{\mu}_j^{min}$, $\boldsymbol{\mu}_j^{max}$). The initial condition is $\boldsymbol{\phi}(0)=\boldsymbol{\psi}(0)$ and $\theta(0)=1$.

In summary, the proposed distributed online algorithm consists of two steps: 1) accelerated dual variable update step (22), and 2) primal variable update steps (16) and (21).

D. Implementation Discussion

Fig. 4 shows the implemented control structure. At each time instant k, based on local measurements and predictions, following the algorithm developed in the first stage, each local control center (LCC) calculates the optimal control sequence of its own OLTC via communication with its neighboring local areas and implements it. However, due to the model inaccuracy and prediction errors in the first stage, the control actions of OLTCs may not fully mitigate the potential voltage violations. In this case, the online controller (described by (16), (21),

and (22)) in the second stage will operate in real-time with a specified sampling period (e.g., 100 ms), and keep processing measurements from the system to produce updates to the set-points of DERs until the voltage violation is mitigated.

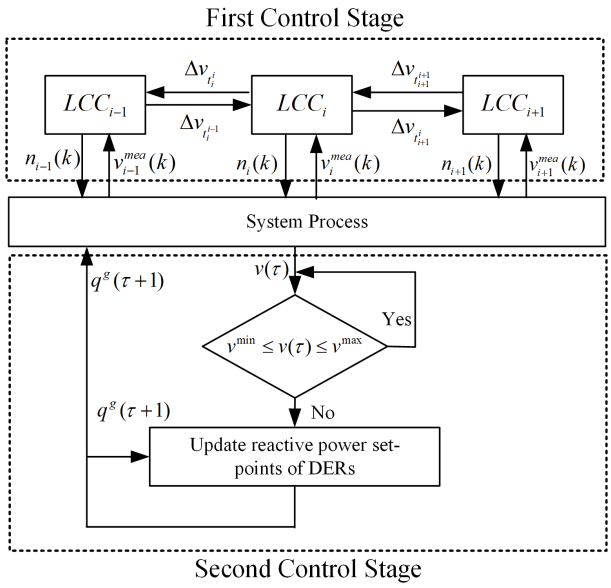

Figure 4: The implementation block diagram

In the proposed voltage control strategy, we assume that each agent (i.e., bus with DER) has the ability of local measurement, calculation, and communicating with its LCC and neighboring agents. This assumption is not harsh for a modern distribution network and has been widely adopted in the literature (e.g. [4]–[6]). If some voltage measurements required in framework are unavailable, they can be estimated online based on the available voltage measurements [25]. How to incorporate this estimation scheme into the proposed control strategy deserves attention and will be studied in future.

IV. Case Study

In this section, two different IEEE test feeders are employed to demonstrate the effectiveness and advantage of the proposed control framework. During the simulation, the nonlinear ac power flow model, instead of the linearized DistFlow model, is used to model the distribution networks.

A. IEEE 34-bus test feeder

Fig. 5 shows the diagram of a modified IEEE 34-bus test feeder [26]. In the modified test system, an ideal OLTC that is connected to the substation bus is added and the resistance of lines are randomly selected such that the R/X ratio ranges from 1 to 2. Without loss of generality, we assume that the bus voltage of substation is fixed to be unity, i.e., $v_S = 1$. If v_S is controllable, it can be incorporated in the proposed model by regarding Δv_S as a decision variable in (5), i.e., $\Delta v_{t_1} = \Delta v_S$. We also assume that there is a PV inverter at each load bus with the capacity of 7 kVA. The whole network is partitioned into three local control areas, i.e. $N_t = 3$.

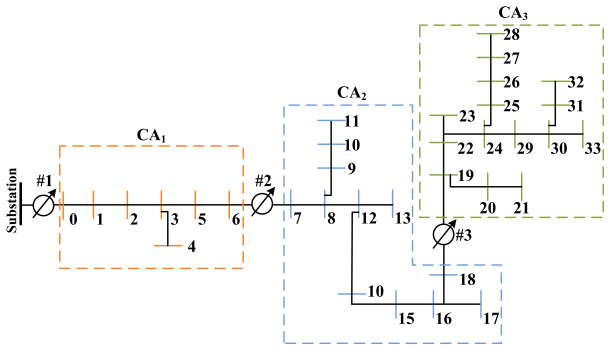

Figure 5: The modified IEEE 34-bus test feeder

During the simulation, all bus voltages in the network are required to be regulated within the nominal range $[0.95, 1.05]$ p.u., i.e., to avoid voltage violations.

To simulate a dynamic scenario, we use real data of a particular day for residential load and solar generation profiles, both at 5-minute resolutions, which are shown in Fig. 6. We also diversify the load and solar generation profile for each bus by small random additive noises. The short-term predicted (10-minute ahead) load and solar generation profiles can be obtained by using a series of advanced forecast tool boxes including *OptiLoad* and *OptiSolar* [27], which are also given in Fig. 6 for controller design in the first stage.

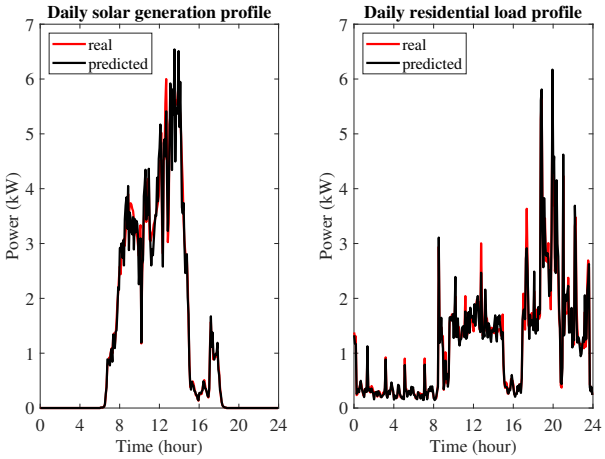

Figure 6: Daily residential active load and solar generation profiles.

The controller used consists of three OLTCs and 33 PV inverters. For OLTCs, the turns ratios can change in 0.01-p.u. steps from 0.90 to 1.10 p.u.. For PV inverters, the reactive power change limits $\underline{q}_j^g$ and $\overline{q}_j^g$ for buses j, $j \in \mathcal{N}_b$ are updated based on the given inverter rating (i.e., 7 kVA) and concurrent solar power generation.

The parameters used in the proposed control framework are given as follows:

1) In the first stage, the sample time period of DMC is chosen as 5 minutes; the controller uses $N_c = N_p = 1$. In the objective function of (6), the weights for tap ratio changes of OLTCs are the same and selected as

$c_i = 1,\ i \in \mathcal{N}_t$, and the cost of using the slack values is 1000 times higher than that of tap ratio changes (i.e., $s_{\varepsilon i} = s_{\delta i} = 1000,\ i \in \mathcal{N}$). In (8), we set the parameter $\rho = 1$. In order to account for the model inaccuracy introduced by model in (6), the voltage control limits in (6d) are set as $[0.96, 1.04]$ p.u. for all buses, which is narrower than the nominal control range.

2) In the second stage, the sample time period is chosen as 100 ms. In the objective function of (11), the weights for slack variables are set as $s_{\varphi i} = s_{\xi i} = 100,\ i \in \mathcal{N}_b$. The voltage control limits in (11b) is set as the nominal voltage range. The step size in (22) is selected as $\gamma = 10^{-4}$.

It should be noted that, during the simulation, the computation time needed in the first stage to obtain the optimal control sequence of OLTCs is around 0.4 s and the calculation time needed to finish one iteration in the second stage is around 3 ms. Compared with the sampling time periods selected, the calculation time needed in both stages are almost trivial.

Scenario 1 – basic effectiveness test

Fig. 7 and Fig. 8 show the daily voltage profile without and with the proposed voltage control framework, respectively. Clearly, the voltage violations have been mitigated by the proposed control framework, which demonstrates the effectiveness of the proposed voltage control strategy. Fig. 9 shows the daily voltage profile only with the first control stage. We can see that the voltage violations cannot be fully mitigated by only the first control stage, which demonstrates the necessity and importance of the second control stage.

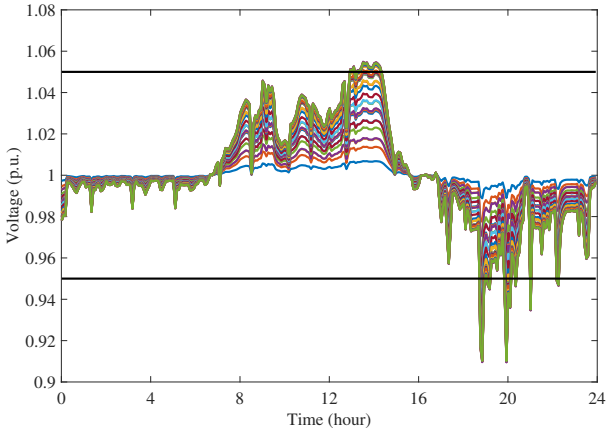

Figure 7: Daily bus voltage profile without control in IEEE 34-bus test feeder.

Fig. 10 shows the continuous and discrete optimal control sequences of three OLTCs, respectively. Fig. 11 shows the online update process of the second stage after the first unmanageable voltage violation is detected at 12 : 39 : 00 PM, where reactive power set-points of all PV inverters keep updated based on real-time voltage measurements at each sampling time instant until the voltage violation is mitigated. Fig. 14a shows the control actions of all PV inverters during the simulation.

Scenario 2 – Comparison with a centralized approach

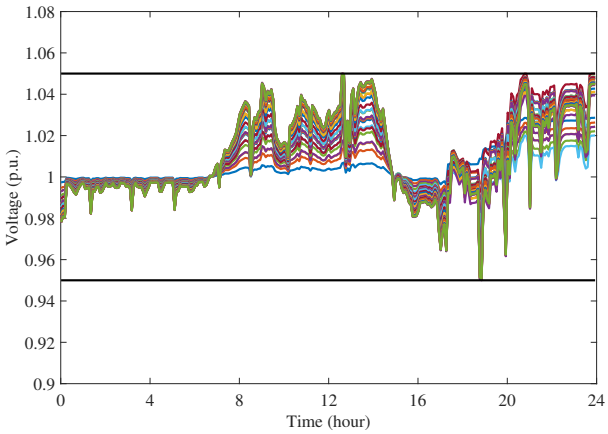

Figure 8: Daily bus voltage profile under control in IEEE 34-bus test feeder.

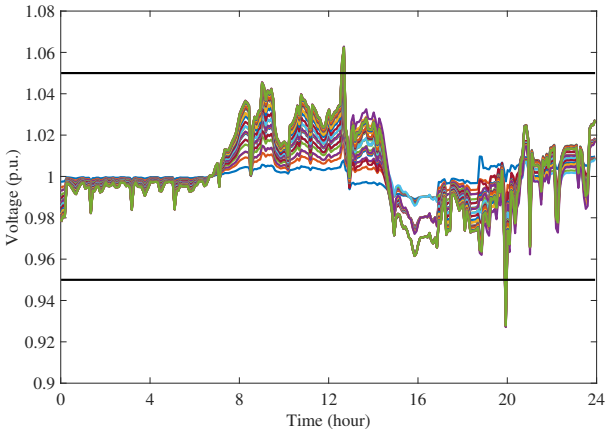

Figure 9: Daily bus voltage profile under first control stage in IEEE 34-bus test feeder.

In order to show the advantage of our control approach, we compare the control performance of the proposed distributed control scheme with that of a centralized scheme. In the centralized scheme, based on the linearized DistFlow model and an approximate voltage relationship of OLTCs developed in (5), following the procedure in [15], the whole control problem is regarded as an integrated (OLTC and DERs) optimal reactive power flow one and formulated as a mixed integer quadratic programming problem. All parameters needed in the centralized scheme are the same as those used in our distributed scheme. Fig. 12 shows the voltage profile obtained under the centralized control scheme. Fig. 13 and Fig. 14 show the control actions needed for the centralized scheme and the proposed distributed approach, respectively. Through comparison, we observe that the centralized approach can obtain optimal control actions but worse control performance (i.e., cannot fully mitigate the voltage violations), whereas the proposed distributed control framework achieves better control performance with sub-optimal solutions.

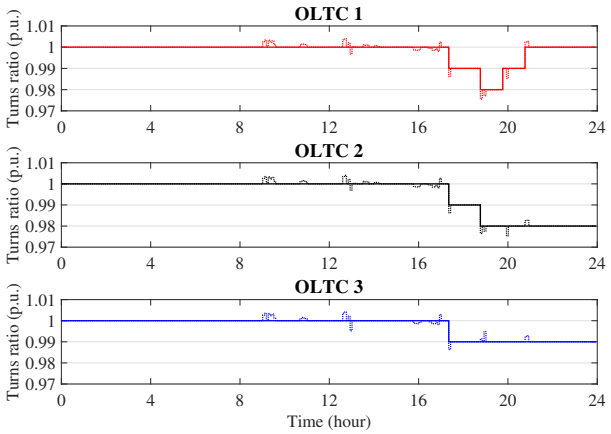

Figure 10: The optimal control actions of OLTCs in IEEE 34-bus test feeder (solid: discrete, dotted: continuous).

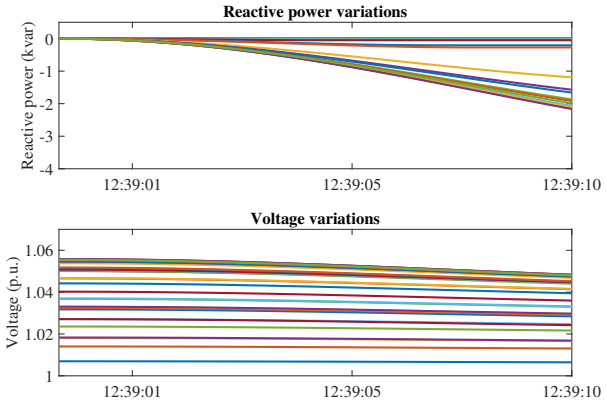

Figure 11: Reactive power injections of PV inverters and corresponding voltage variations

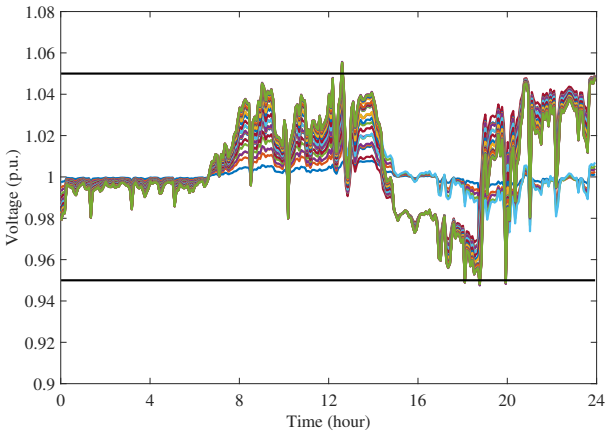

Figure 12: Daily bus voltage profile under centralized control in IEEE 34-bus test feeder.

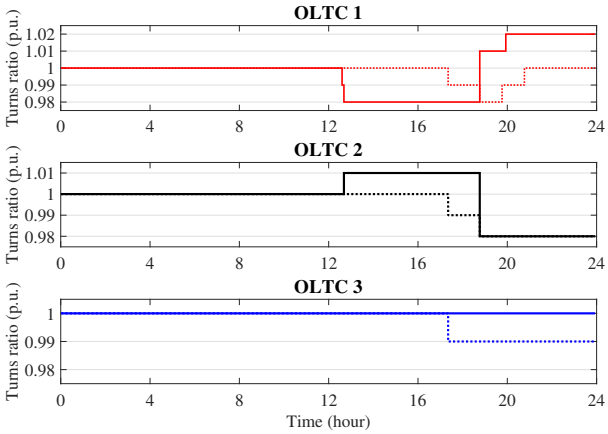

Figure 13: The optimal control actions of OLTCs in IEEE 34-bus test feeder (solid: centralized, dotted: distributed).

B. IEEE 123-bus test feeder

We now test the proposed control framework in a large test feeder, i.e., a modified IEEE 123-bus test feeder [26], whose diagram is shown in Fig. 15. In the modified system, again, we assume that the bus voltage of the substation is fixed to be unity, i.e., $v_S = 1$. We also assume that there is a PV inverter at each load bus with the capacity of 7 kVA. The whole network is partitioned into four local control areas, i.e. $N_t = 4$.

During the simulation, the control objective is still to regulate all bus voltages in the network within the nominal range [0.95, 1.05] p.u.. To simulate the dynamic scenario, the load and solar generation files shown in Fig. 6 are employed again and diversified by small random additive noises for each bus. The controller used here consists of four OLTCs and 122 PV inverters. The control parameters used are the same as those employed in the modified 34-bus test feeder.

Fig. 16 and Fig. 17 show the daily voltage profile without and with the proposed voltage control method, respectively. Through comparison, it is clear that the voltage violations are mitigated effectively by the proposed control framework, which demonstrates the effectiveness and scalability of the proposed scheme. Fig. 18 shows the daily voltage profile only with the first control stage. We observe that the voltage violations cannot be fully mitigated by only the first control stage, which demonstrates the necessity and importance of the second control stage again. Fig. 19 shows the control actions of OLTCs during the simulation.

V. Conclusion

This paper has proposed a distributed coordinated voltage control framework to handle uncertain voltage violations in active distribution networks. The proposed control framework consists of two stages that work in a complementary manner. In the first stage, with the help of load and renewable predictions, the OLTCs have been utilized to handle the potential voltage violations via the proposed DMC framework. However, due to the control inaccuracy of the first stage, the voltage violation may not be fully avoided. To handle this issue, the reactive powers of DERs have been coordinated in the second stage via the proposed online distributed algorithm to bring the voltages within their allowable limits. The effectiveness of the proposed control framework has been verified through different standard test feeders.

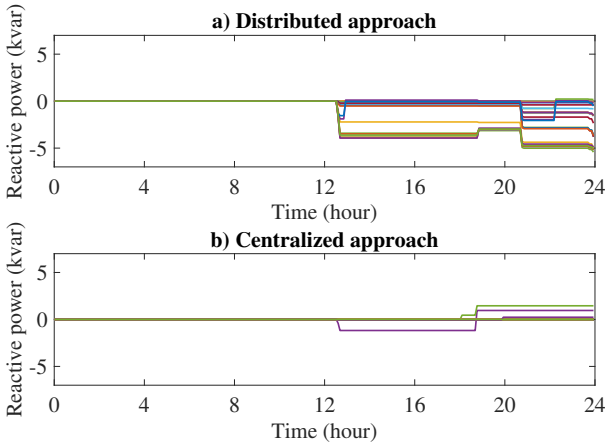

Figure 14: The control actions of PV inverters in IEEE 34-bus test feeder

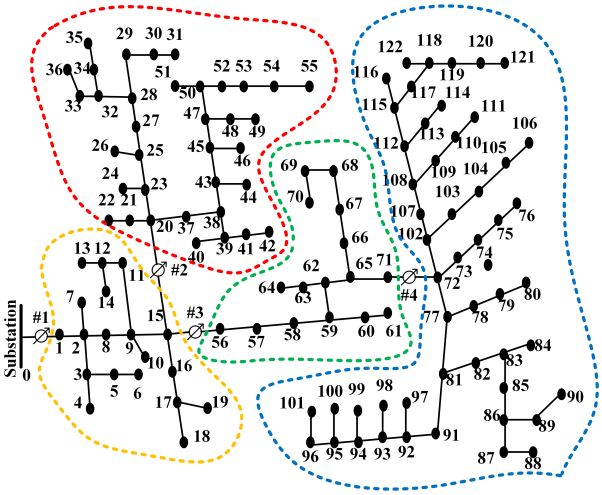

Figure 15: The modified IEEE 123-bus test feeder

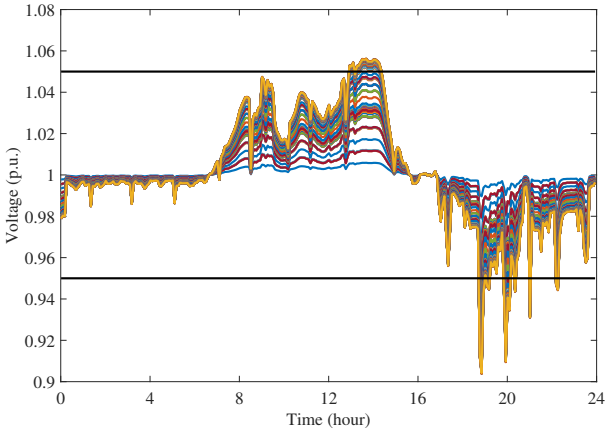

Figure 16: Daily bus voltage profile without control in IEEE 123-bus test feeder.

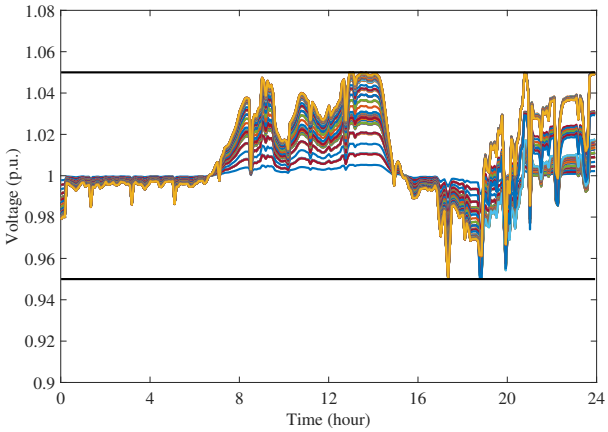

Figure 17: Daily bus voltage profile under control in IEEE 123-bus test feeder.

REFERENCES

[1] K. Turitsyn, P. Sulc, S. Backhaus, and M. Chertkov, "Options for control of reactive power by distributed photovoltaic generators," *Proceedings of the IEEE*, vol. 99, no. 6, pp. 1063-1073, Jun. 2011.

[2] H. Zhu and H. J. Liu, "Fast local voltage control under limited reactive power: Optimality and stability analysis," *IEEE Trans. Power Syst.*, vol. 31, no. 5, pp. 3794-3803, Sep. 2016.

[3] G. Valverde and T. Van Cutsem, "Model predictive control of voltages in active distribution networks," *IEEE Trans. Smart Grid*, vol. 4, no. 4, pp. 2152-2161, Dec. 2013.

[4] H. S. Bidgoli and T. Van Cutsem, "Combined local and centralized voltage control in active distribution networks," *IEEE Trans. Power Syst.*, vol. 33, no. 2, pp. 1374-1384, Mar. 2018.

[5] H. J. Liu, W. SHi, and H. Zhu, "Distributed voltage control in distribution networks: Online and robust implementations," *IEEE Trans. Smart Grid*, vol. 9, no. 6, pp. 6106-6117, Nov. 2017.

[6] B. Robbins, C. N. Hadjicostis, and A. D. Dominguez-Garcia, "A two-stage distributed architecture for voltage control in power distribution systems," *IEEE Trans. Power Syst.*, vol. 28, no. 2, pp. 1470-1482, May 2013.

[7] K. Baker, A. Bernstein, E. Dall'Anese, and C. Zhao, "Network-cognizant voltage droop control for distribution grids," *IEEE Trans. Power Syst.*, vol. 33, no. 2, pp. 2098-2108, Mar. 2018.

[8] M. Farivar, L. Chen, and S. Low, "Equilibrium and dynamics of local voltage control in distribution systems," In *Proc. IEEE 52nd Conf. Decision and Control (CDC)*, pp. 4329-4334, 2013.

[9] V. Kekatos, L. Zhang, G. B. Giannakis, and R. Baldick, "Voltage regulation algorithms for multiphase power distribution grids," *IEEE Trans. Power Syst.*, vol. 31, no. 5, pp. 3913-3923, Sep. 2016.

[10] P. N. Vovos, A. E. Kiprakis, A. R. Wallace, and G. P. Harrison, "Centralized and distributed voltage control: Impact on distributed generation penetration," *IEEE Trans. Power Syst.*, vol. 22, no. 1, pp. 476-483, Feb. 2007.

[11] P. Carvalho, P. F. Correia, and L. A. Ferreira, "Distributed reactive power generation control for voltage rise mitigation in distribution networks," *IEEE Trans. Power Syst.*, vol. 23, no. 2, pp. 766–772, May 2008.

[12] P. Šulc, S. Backhaus, and M. Chertkov, "Optimal distributed control of reactive power via the alternating direction method of multipliers," *IEEE Trans. Energy Convers.*, vol. 29, no. 4, pp. 968-977, Dec. 2014.

[13] S. Bolognani, R. Carli, G. Cavraro, and S. Zampieri, "Distributed reactive power feedback control for voltage regulation and loss minimization," *IEEE Trans. Autom. Control*, vol. 60, no. 4, pp. 966-981, Apr. 2015.

[14] Z. Tang, D. J. Hill, T. Liu, and H. Ma, "Hierarchical voltage control of weak subtransmission networks with high penetration of wind power," *IEEE Trans. Power Syst.*, vol. 33, pp. 187-197, Jan. 2018.

[15] Y. Xu, Z. Y. Dong, R. Zhang, and D. J. Hill, "Multi-timescale coordinated voltage/var control of high renewable-penetrated distribution systems," *IEEE Trans. Power Syst.*, vol. 32, no. 6, pp. 4398-4408, Nov. 2017.

[16] R. Zafar, J. Ravishankar, J. E. Fletcher, and H. R. Pota, "Multi-timescale model predictive control of battery energy storage system using conic relaxation in smart distribution grids," *IEEE Trans. Power Syst.*, vol. 33, no. 6, pp. 7152-7161, Nov. 2018.

[17] C. A. Ferreira and R. B. Prada, "Improved model for tap-changing

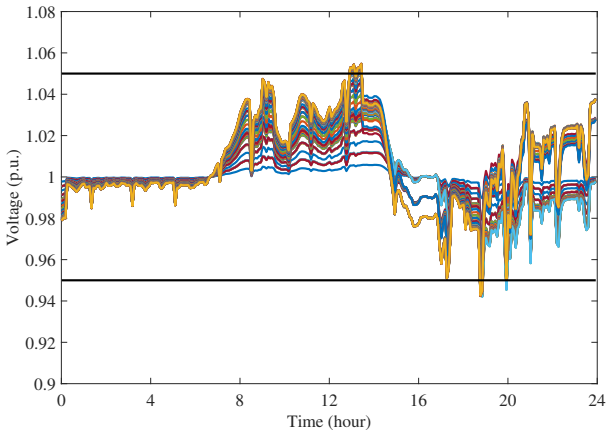

Figure 18: Daily bus voltage profile under first control stage in IEEE 123-bus test feeder.

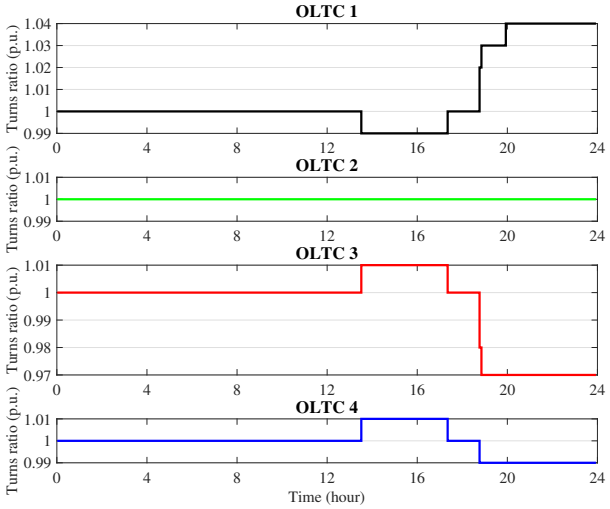

Figure 19: The control actions of OLTCs in IEEE 123-bus test feeder

transformer," *IET Gen., Trans., Dist.*, vol. 7, no. 11, pp. 1289-1295, Nov. 2013.

[18] W. Wu, Z. Tian, and B. Zhang, "An exact linearization method for OLTC of transformer in branch flow model," *IEEE Trans. Power Syst.*, vol. 32, no. 3, pp. 2475-2476, May 2017.

[19] B. A. Robbins, H. Zhu, and A. D. Domínguez-García, "Optimal tap setting of voltage regulation transformers in unbalanced distribution systems," *IEEE Trans. Power Syst.*, vol. 31, no. 1, pp. 256-267, Jan. 2016.

[20] M. E. Baran and F. F. Wu, "Optimal sizing of capacitors placed on a radial distribution system," *IEEE Trans. Power Del.*, vol. 4, no. 1, pp. 735-743, Jan. 1989.

[21] S. Boyd, N. Parikh, E. Chu, B. Peleato, and J. Eckstein, "Distributed optimization and statistical learning via the alternating direction method of multipliers," *Foundations Trends in Mach. Learn.*, vol. 3, no. 1, pp. 1-122, Jan. 2011.

[22] D. P. Bertsekas, "Nonlinear programming," *Journal of the Operational Research Society*, vol. 48, no. 3, pp. 334-334, Mar. 1997.

[23] A. Beck and M. Teboulle, "A fast iterative shrinkage-thresholding algorithm for linear inverse problems," *SIAM J. Img. Sci.*, vol. 2, no. 1, pp. 183-202, Mar. 2009.

[24] Z. Tang, D. J. Hill, and T. Liu, "Fast distributed reactive power control for voltage regulation in distribution networks," *IEEE Trans. Power Syst.*, vol. 34, no. 1, pp. 802-805, Jan. 2019.

[25] E. B. Alzate, M. Bueno, X. Jian, and K. Strunz, "Distribution system state estimation to support coordinated voltage-control strategies by using smart meters," In *IEEE Trans. Power Syst.*, vol. 34, no. 6, pp. 5198–5207, Nov. 2019.

[26] "IEEE PES Distribution Test Feeders," [Online]. Available: https://site.ieee.org/pes-testfeeders/resources/

[27] Y. Zheng, Z. Y. Dong, F. J. Luo, K. Meng, J. Qiu, and K. P. Wong, "Optimal allocation of energy storage system for risk mitigation of DISCOs with high renewable penetrations," *IEEE Trans. Power Syst.*, vol. 29, no. 1, pp. 212-220, Jan. 2014.

Zhiyuan Tang (S'16-M'18) received the B.S. degree in electrical engineering from Xi'an Jiaotong University, Xi'an, China, in 2014 and the Ph.D. degree in power system from the University of Hong Kong (HKU), Hong Kong, in 2018. From September 2018 to July 2019, he was a Senior Research Assistant in HKU. Currently, he is working as a Postdoctoral Fellow in University of Waterloo, Canada. His research interests are in distributed optimal control and its application in power systems especially frequency and voltage control with high renewables.

David J. Hill (S'72-M'76-SM'91-F'93-LF'14) received the PhD degree in Electrical Engineering from the University of Newcastle, Australia, in 1976. During 2013-2020, he held the Chair of Electrical Engineering and was Director of the Centre for Electrical Energy Systems in the Department of Electrical and Electronic Engineering at the University of Hong Kong. Since 2020, he is a part-time Professor in the School of Electrical Engineering and Telecommunications, The University of New South Wales, Sydney, Australia.

He has previously held positions at the University of Sydney including the Chair of Electrical Engineering during 1994-2002 and again in 2010-2013 along with an Australian Research Council Professorial Fellowship. He was Foundation Director of Centre for Future Energy Networks during 2010-2018 and part-time Professor 2013-2020. During 2005-2010, he was an ARC Federation Fellow at the Australian National University. He has also held academic and substantial visiting positions at the universities of Melbourne, California (Berkeley), Newcastle (Australia), Lund (Sweden), Munich and in Hong Kong (City and Polytechnic Universities).

His general research interests are in energy systems, control systems, complex networks, learning systems and stability analysis. His work is now mainly on control and planning of future energy and power networks with some attention to basic stability and control questions for dynamic networks and systems.

Professor Hill is a Fellow of the Society for Industrial and Applied Mathematics, USA, the International Federation of Automatic Control, the Australian Academy of Science, the Australian Academy of Technological Sciences and Engineering and the Hong Kong Academy of Engineering Sciences. He is also a Foreign Member of the Royal Swedish Academy of Engineering Sciences.

Tao Liu (M'13) received his B.E. degree from Northeastern University, China, in 2003 and Ph.D. degree from the Australian National University (ANU), Australia, in 2011. From 2012 to 2015, he had worked as a Post-doctoral Fellow in ANU, University of Groningen, and University of Hong Kong (HKU). He became a Research Assistant Professor in 2015 in HKU where he is an Assistant Professor now. His research interests include power system analysis and control, complex dynamical networks, distributed control, and event-triggered control.